Mesoporous Metals

International Edition: DOI: 10.1002/anie.201603967
German Edition: DOI: 10.1002/ange.201603967

Tunable-Sized Polymeric Micelles and Their Assembly for the Preparation of Large Mesoporous Platinum Nanoparticles

Bo Jiang, Cuiling Li, Jing Tang, Toshiaki Takei, Jung Ho Kim, Yusuke Ide, Joel Henzie, Satoshi Tominaka, and Yusuke Yamauchi**

Abstract: *Platinum nanoparticles with continuously tunable mesoporous structures were prepared by a simple, one-step polymeric approach. By virtue of their large pore size, these structures have a high surface area that is accessible to reagents. In the synthetic method, variation of the solvent composition plays an essential role in the systematic control of pore size and particle shape. The mesoporous Pt catalyst exhibited superior electrocatalytic activity for the methanol oxidation reaction compared to commercially available Pt catalysts. This polymeric-micelle approach provides an additional design concept for the creation of next generation of metallic catalysts.*

Micelle architectures provide a simple and versatile platform for the synthesis of mesoporous structures in a wide variety of materials.[1] Both pore size and the porous structure of the materials can be controlled by tuning the inter- and intramolecular forces that drive the self-assembly of surfactants and block copolymers.[2] Mesoporous materials with large pore sizes have inspired a wide variety of applications because large pores facilitate fast and efficient transport of reactants.[3] For example, Zhao and co-workers reported that three-dimensional (3D) ordered mesoporous silica with ultralarge accessible mesopores can be synthesized on high-molecular-weight block-copolymer templates. They used solvent evaporation to make composite micelles composed of a block copolymer and a silica precursor to assemble the ordered mesostructure.[4] Although the synthesis of these large-pore materials have been demonstrated, their compositions are still limited to carbon,[5] silica,[4,6] metal oxides,[7] and organosilicates.[8] If these micelle templates could be applied to the preparation of noble metals, in particular, materials such as platinum, these ultralarge accessible surfaces would be of great utility for electrocatalysis.

Mesoporous noble-metal materials (e.g., Au, Pt, Pd) have most of the physical and chemical properties that make these metals good catalysts. Consequently, these structures exhibit enhanced catalytic properties for a range of reactions, including small-organic-molecule oxidation, the oxygen reduction reaction, and hydrogenation.[9] Our previous studies demonstrated that mesostructured noble metals with large pores could be synthesized by using pore-directing agents, such as the block copolymer polystyrene-*block*-poly(ethylene oxide) (PS-*b*-PEO), through electrochemical deposition.[10] However, this method required the metal species to be electrodeposited on conductive substrates, limiting the obtained materials primarily to monolith films. Chemical reduction might provide a more flexible way to make metal nanoparticles in solution.[11] To our knowledge, chemical reduction has never been used for the controlled synthesis of large-sized porous metallic nanoparticles with tunable pore sizes and particle sizes. Consequently, new synthetic strategies must be developed to enable the reduction of metal species on block-copolymer micelles to create nanoparticles with large, open pores as high-performance electrocatalysts.

Herein we report a simple micelle-based approach to make mesoporous Pt nanoparticles. By controlling the solvent composition, we are able to make nanoparticles with continuously tunable porous architectures and particle sizes (Figure 1). The Pt precursor is chemically reduced by ascorbic acid in a mixture of tetrahydrofuran (THF) and water. The concept of our approach is different from that of traditional micelle systems prepared by dialysis and solvent evaporation,[12] because the addition of water induces the micellization of block copolymers. The solubility of the hydrophobic blocks depends on the tetrahydrofuran content, so micelle size can be tuned by varying the THF content to create a fully tunable mesoporous Pt nanoparticle system. The as-prepared mesoporous Pt nanoparticles are referred to herein as Pt-*x*-(100-*x*), where *x* represents the percentage (v/v %) of THF in the precursor solutions. The electrochemical performance of the mesoporous Pt structures was carefully examined and showed a great improvement over conventional platinum catalysts, thus demonstrating that the mesoporous design is a route to better catalytic activity.

The hydrophilic and hydrophobic segments of the diblock polymer poly(ethylene oxide)-*b*-poly(methyl methacrylate) (PEO-*b*-PMMA) have similar solubility parameters in THF.[13] The addition of water causes the hydrophobic PMMA segments to become less solvated, so that spherical micelles are formed that are composed of the PMMA block as

[*] B. Jiang, Dr. C. Li, J. Tang, Dr. T. Takei, Dr. Y. Ide, Dr. J. Henzie, Dr. S. Tominaka, Prof. Y. Yamauchi
Mesoscale Materials Chemistry Group
International Center for Materials Nanoarchitectonics (MANA)
National Institute for Materials Science (NIMS)
1-1 Namiki, Tsukuba, Ibaraki 305-0044 (Japan)
E-mail: LI.Cuiling@nims.go.jp
Yamauchi.Yusuke@nims.go.jp
B. Jiang, J. Tang, Prof. Y. Yamauchi
Faculty of Science and Engineering, Waseda University
3-4-1 Okubo Shinjuku, Tokyo 169-8555 (Japan)
Prof. J. H. Kim, Prof. Y. Yamauchi
Australian Institute for Innovative Materials (AIIM)
University of Wollongong
Squires Way, North Wollongong, NSW 2500 (Australia)

Supporting information for this article can be found under: http://dx.doi.org/10.1002/anie.201603967.

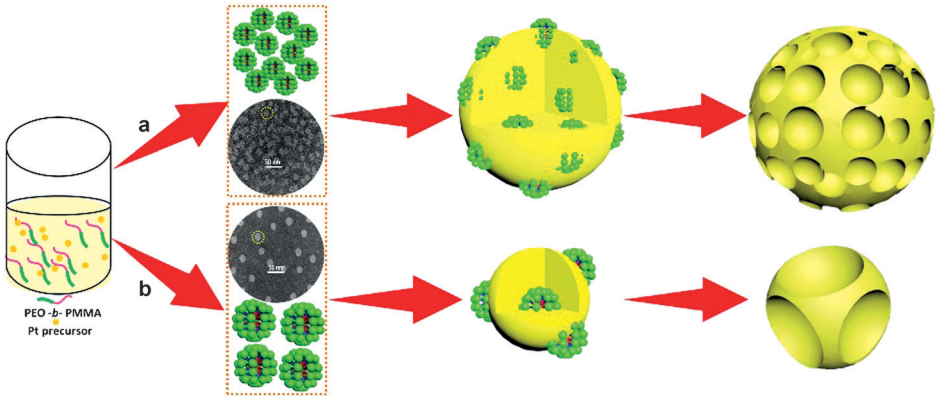

Figure 1. Process for the formation of a) mesoporous Pt-8-92 at a low THF content, and b) dimpled Pt-14-86 nanoparticles at a high THF content (scale bars: 50 nm).

a core surrounded by a PEO shell, as illustrated by the Tyndall effect (see Figure S1 in the Supporting Information). In aqueous solution, the $[PtCl_4]^{2-}$ ions are coordinated by water molecules to form platinum–water complexes.[14] Previous studies demonstrated that such coordinated complexes can be incorporated inside the ethylene oxide (EO) shells of the polymeric micelles by hydrogen bonding.[15] During the deposition of Pt, the PEO-*b*-PMMA micelles act as templates to form the mesoporous structure.

The structural features of the mesoporous Pt nanoparticles were characterized by scanning electron microscopy (SEM; Figure 2). Both the porous structure and the particle size depend on the solvent composition (herein, the volume ratio between THF and H_2O). The Pt-4-96, Pt-6-94, and Pt-8-92 samples prepared from 4:96, 6:94, and 8:92 THF/H_2O had a dense assemblage of mesopores packed inside the spheres (Figure 2a–c). The porous structures gradually transformed into dimpled mesopores as the THF/H_2O volume ratio increased to 14:86 (Figure 2e,f). As the THF/H_2O volume ratio changed from 4:96 to 6:94, 8:92, 10:90, 12:88, and 14:86, we observed a corresponding decrease in particle size from (107 ± 1) nm to (86 ± 1), (62 ± 1), (46 ± 1), (37 ± 1), and (32 ± 1) nm, while the pore size of the samples increased slightly from (8 ± 0.5) nm to (9 ± 0.5), (10 ± 0.5), (12 ± 0.5), (14 ± 0.5), and (14 ± 0.5) nm, respectively (see Figure S2). These statistical results were estimated from the SEM images. The above result (see Figure S3) demonstrates that the solvent composition plays a key role in the variation of the pore size and the particle size, and ultimately determines the mesoporous structure of the nanoparticles.

Mesoporous Pt-8-92 nanoparticles were investigated in detail with a combination of electron microscopy and X-ray characterization techniques. SEM and transmission electron microscopy (TEM) images of the particles prove that the densely packed spherical mesopores are distributed not only on their surfaces but also inside the nanoparticles (Figure 3). Low-angle X-ray diffraction (XRD) is a better way to determine the periodicity (i.e., pore-to-pore distance) of the mesoporous structure in the entire ensemble of particles. The measurement shows a broad peak located at 0.55° ($d =$ 16.0 nm), which corresponds to the expected pore-to-pore distance of the mesoporous structure (see Figure S4a). The wide-angle XRD pattern of the obtained sample displays five pure Pt peaks, which can be assigned as (111), (200), (220), (311), and (222) diffraction peaks, respectively (Figure S4b). Closer examination of the individual nanoparticles by high-resolution TEM (HRTEM) showed that the pore walls are composed of numerous small interconnected nanoparticles (ca. 4–6 nm; see Figure S5). Polycrystallinity was confirmed by the selected area electron diffraction (SAED) pattern (see Figure S5b), which showed concentric rings composed of bright discrete diffraction spots that can be assigned to a face-centered-cubic (*fcc*) Pt crystal for individual particles. The HRTEM image taken from the edge of the particle had a lattice spacing of 0.23 nm, which corresponds to the *fcc* Pt(111) crystal plane (see Figure S5d). The average grain size is approximately 9 nm, as calculated from the XRD diffraction peaks (see Figure S4b) on the basis of the Scherrer equation. Therefore, the crystallinity is extended over a couple of nanoparticles.

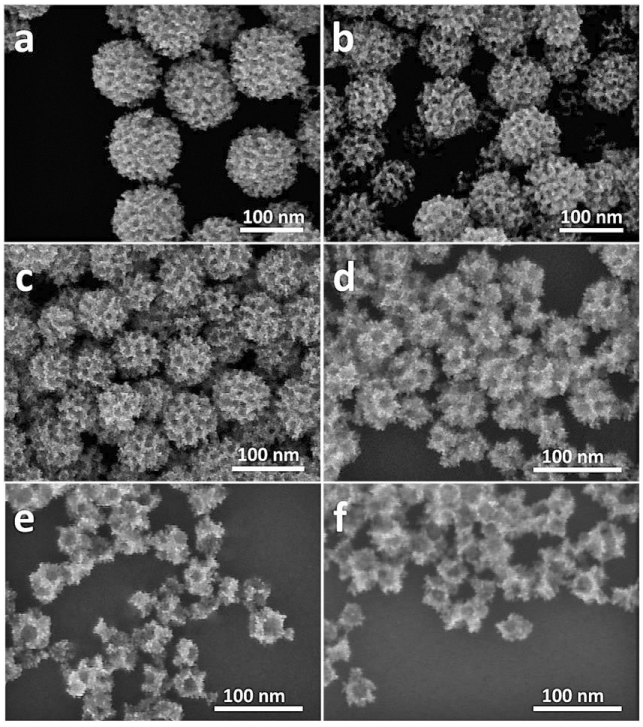

Figure 2. SEM images of mesoporous a) Pt-4-96, b) Pt-6-94, c) Pt-8-92, d) Pt-10-90, e) Pt-12-88, and f) Pt-14-86 samples prepared from THF/H_2O solvent mixtures with various volume ratios [a) 4:96, b) 6:94, c) 8:92, d) 10:90, e) 12:88, and f) 14:86].

We examined the mesoporous Pt-14-86 nanoparticles synthesized at a higher THF concentration to understand the influence of the solvent composition. The sample was highly dispersed, with a narrow particle-size distribution, and dimple-like pores (see Figure S6a). Interestingly, the size of the nanoparticle was smaller, whereas the pores on the

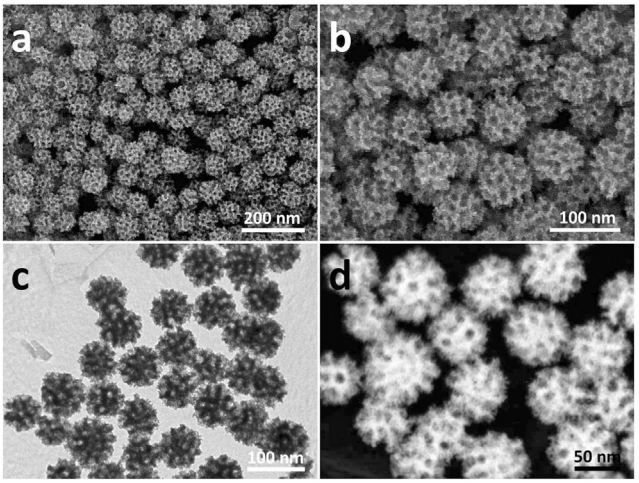

Figure 3. a,b) Low- and high-magnification SEM, c) TEM, and d) HAADF-STEM images of the Pt-8-92 sample prepared by using a THF/H_2O volume ratio of 8:92.

surface were larger and less numerous. Electron microscopy revealed that each nanoparticle possessed 1–2 central spherical pores, and several small branches around its exterior (see Figure S6). The particle size and shape are directly related to the solvent composition (Figure 2; see also Figure S2).

In this study, solvent composition had a large impact on the final Pt structure, so we attempted to observe this effect directly in the polymeric micelles themselves. The polymeric micelles formed at THF/H_2O various volume ratios were stained with phosphotungstic acid (1.0 wt%) and studied by TEM. Spherical micelles were formed in the THF/H_2O solvent mixtures (see Figure S7). In the TEM images, the bright spheres correspond to the micelles (regions of lower electron density) owing to the negative staining by phosphotungstic acid.[16] The micelle size increased from (14 ± 0.5) to (17 ± 0.5) and (19 ± 0.5) nm as the THF/H_2O volume ratio increased from 8:92 to 10:90 and 14:86. This change in the micelle size is probably due to the solubility change of the hydrophobic PMMA block in the mixed solvents. Exactly as observed for our mesoporous Pt nanoparticles, a larger amount of THF caused the PMMA blocks to swell, thus leading to an expansion of the size of the pores in the Pt nanoparticles (see Figures S1 and S2).

It must be considered that the THF content in the PEO-*b*-PMMA solution could affect the number of free unimers and micelles in the solution. At a lower THF content, the fraction of micelles is increased, because the block polymer tends to form micelles in a high volume ratio of water to THF.[4,17] This high micelle concentration facilitates the ready assembly of a large number of micelles (Figure 1a), resulting in large-sized spherical particles (Figure 2a,b). On the other hand, at higher THF content, swollen micelles are formed, and their micelle concentration is decreased (Figure 1b), which favors the formation of smaller-sized Pt particles with enlarged pores (Figure 2e,f). Our results are consistent with a previous study on mesoporous silica, in which a high THF concentration promoted the formation of hollow structures by isolated micelles, whereas a low THF concentration resulted in the formation of mesoporous structures derived from a large number of well-packed micelles.[4] When the THF concentration was increased even more (THF/H_2O 16:84), hemispherical Pt nanoparticles with a few enlarged pores on the surface were observed (see Figure S8). To our knowledge, tuning of the size of particles, the number of pores on their surface, and the pore size by simply changing the solvent composition has not been reported previously. We believe that this concept provides a new way to construct the internal structure of metallic nanoparticles. To investigate the growth of Pt particles in the solution phase, we observed the intermediate products at different reaction times by TEM (see Figure S9). The Pt precursor was first reduced to tiny nanocrystals, which were likely stabilized by the EO chains of the micelles. As the reaction proceeded, the tiny crystals grew larger and began to coat on the spherical PEO-*b*-PMMA micelles. After 100 min, the mesoporous structures started to form.

In the present synthesis, the use of the hydrophobic PMMA block in PEO-*b*-PMMA was critical for the formation of mesoporous Pt nanoparticles. When $PEO_{(10500)}$-*b*-$PMMA_{(18000)}$ was replaced with a block polymer with a rigid hydrophobic block (for example, $PEO_{(7500)}$-*b*-$PS_{(18000)}$), a turbid solution instead of a transparent solution was obtained under the same conditions (see Figure S10a). A large amount of THF was necessary to obtain a transparent solution of $PEO_{(7500)}$-*b*-$PS_{(18000)}$, but exclusively resulted in Pt aggregates (see Figure S10b), which is different from our previous electrochemical deposition system.[10] We concluded that the PMMA blocks in PEO-*b*-PMMA are more flexible and weakly hydrophobic as compared to the PS blocks in the PEO-*b*-PS. Furthermore, the pore size of the nanoparticles can be readily tuned by changing the molecular weight of the PMMA block. Thus, the pore size increased from (10 ± 0.5) to 15 ± 0.5 nm when the block copolymer was changed from $PEO_{(10500)}$-*b*-$PMMA_{(18000)}$ to $PEO_{(10500)}$-*b*-$PMMA_{(22000)}$ (see Figure S11b,c). On the other hand, (5 ± 0.5) nm dendritic-like pores were formed when $PEO_{(10500)}$-*b*-$PMMA_{(18000)}$ was replaced with $PEO_{(15000)}$-*b*-$PMMA_{(9000)}$ (see Figure S11a).

Electrocatalytic activity depends on both the particle size and the porous structure of Pt nanoparticles. We examined the activity of the mesoporous Pt nanoparticles for the methanol oxidation reaction (MOR). For comparison with the performance of commercially available catalysts (Pt black is abbreviated as PtB whereas 20 wt% Pt supported on carbon is abbreviated as PtC-20%), all the mesoporous Pt nanoparticles were deposited on a carbon support (Ketjen black, abbreviated as KB) with a mass loading amount of 20% by sonicating a mixture of mesoporous Pt nanoparticles and KB in ethanol/water. This procedure was followed by washing several times with ethanol and water. Finally, the samples were calcinated in air at 250°C to completely remove the block copolymer and other contamination, leaving the mesoporous Pt structure (see Figure S12). The electrochemical surface area (ECSA) of all the samples was measured by cyclic voltammetry in 0.5 M H_2SO_4 solution (see Figure S13a). PtB and PtC-20% were characterized under the same conditions as the mesoporous Pt nanoparticles. Clear features of hydrogen and oxygen adsorption/desorption on the mesoporous Pt catalyst are indications of the cleanliness of the

catalyst surface. The ECSA was calculated by integrating the charge passed in the hydrogen-adsorption/desorption regions, whereby a value of 210 $\mu C\,cm^{-2}$ was assumed for the adsorption of a hydrogen monolayer.[18] The ECSA value was 32 $m^2\,g^{-1}$_Pt for mesoporous Pt-8-92, 15 $m^2\,g^{-1}$_Pt for PtB, and 55 $m^2\,g^{-1}$_Pt for PtC-20%. The ECSA of mesoporous Pt nanoparticles was lower than that of the commercial PtC-20% (ca. 4 nm), probably because the tiny nanoparticles are connected in the mesoporous structure.

Typical cyclic voltammetric curves for MOR catalyzed by the three catalysts in 0.5 M H_2SO_4 solution containing 0.5 M methanol at a scan rate of 50 $mV\,s^{-1}$ are shown in Figure 4a,b. The characteristic methanol oxidation peaks were identified in the forward and backward scans.[19] The peak current of mesoporous Pt-8-92 (405 $mA\,mg^{-1}$_Pt) in the forward sweep was higher than that of the commercial PtC-20% (235 $mA\,mg^{-1}$_Pt) and PtB catalysts (68 $mA\,mg^{-1}$_Pt). Even when the activities were normalized according to the ECSA, the mesoporous Pt-8-92 nanoparticles still exhibited the best catalytic activity toward MOR (1.29 $mA\,cm^{-2}$). It was much higher than that of the PtC-20% (0.5 $mA\,cm^{-2}$) and PtB catalysts (0.4 $mA\,cm^{-2}$). Additionally, the mesoporous Pt nanoparticles exhibited a negatively shifted onset potential for MOR, thus indicating that the oxidation of methanol was easier to be triggered on its surface.[20] Such improved catalytic activity of the mesoporous Pt-8-92 nanoparticles can be ascribed to 3D accessible mesoporous structure.[21] As compared to previously reported platinum-based catalysts (see Table S1 in the Supporting Information), our mesoporous Pt-8-92 nanoparticles exhibited a higher current density.

The dependence of catalytic activity on pore size and nanoparticle size was further studied by comparing the performances of the mesoporous Pt nanoparticles (see Table S2). We found that the catalytic activity of samples depended on the measured ECSAs, which depend on both the nanoparticle size and the pore size. As the particle size decreased (to (62 ± 1) nm), the mass activity gradually increased up to 405 $mA\,mg^{-1}$_Pt owing to the increased ECSAs. However, further decrease in the particle size results in a smaller ECSA value, because the pore size increases, whereas the number of pores on the surface decreases. We concluded that larger mesopores, or fewer of them, result in a smaller ESCA value and ultimately lead to a loss in mass activity.

The chronoamperometric data recorded at 0.6 V for 3000 s showed that the mesoporous Pt nanoparticles possessed a good retention and a higher current density than those of the PtC-20% and PtB catalysts (Figure 4c). The structural stability of our mesoporous Pt nanoparticles is well-supported because the ECSA is retained after cycling treatment. The mesoporous Pt nanoparticles lost only 15% of the initial Pt ECSA, whereas the commercial PtC-20% and PtB lost 55 and 60% of their initial ECSA, respectively (see Figures S3d and S13b–d). We believe that the mesoporous structure has higher stability because it is less vulnerable to aggregation (see Figure S14).[22]

In summary, we have developed a novel method to synthesize continuously tunable mesoporous nanoparticles using polymeric micelles and chemical reduction. We could not observe any irregularly shaped or nonporous Pt particles (see Figure S15), thus highlighting our high-yielding synthesis. The essence of this approach is to utilize the composition of the solvent to selectively vary the solubility of the micelles which changes their size. Continuously tunable porous structures are important for the future design of porous materials with superior catalytic activities.

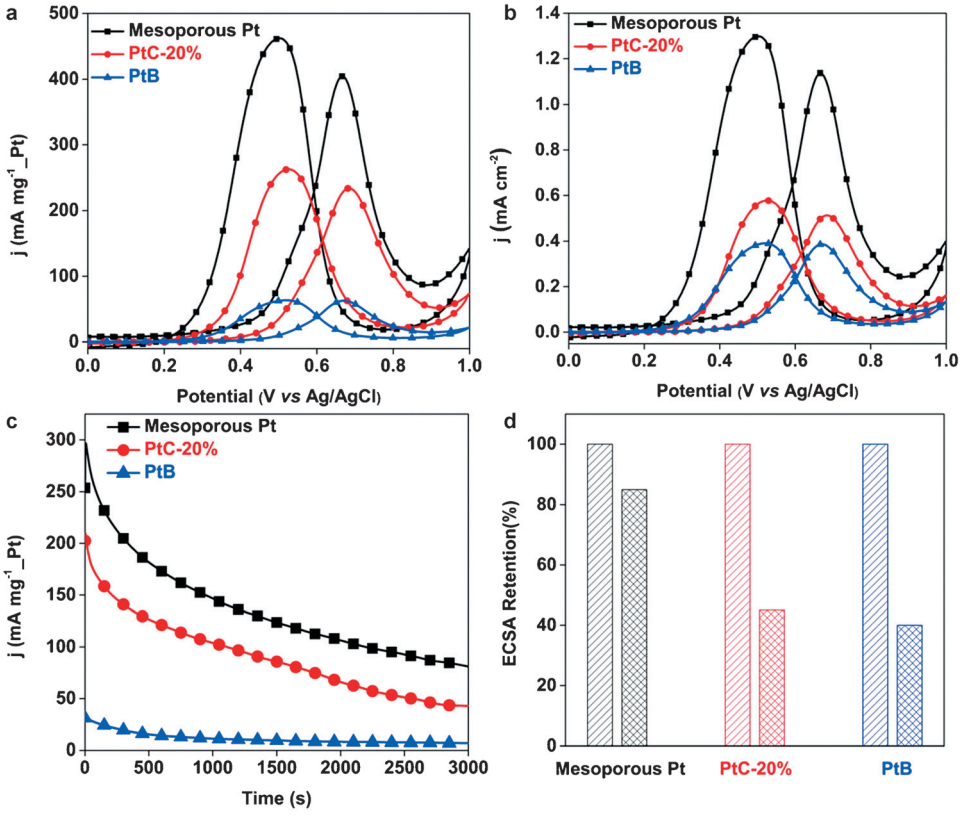

Figure 4. Comparison of mesoporous Pt nanoparticles with commercial catalysts. a) Mass-normalized cyclic voltammograms, b) ECSA-normalized cyclic voltammograms, and c) mass-normalized chronoamperometric curves (recorded at 0.6 V) for methanol oxidation reactions catalyzed by the Pt-8-92 catalyst, commercial PtB catalyst, and PtC-20% catalyst in 0.5 M H_2SO_4 + 0.5 M CH_3OH. d) Comparison of ECSA retention of the Pt-8-92 catalyst, commercial PtB catalyst, and PtC-20% catalyst after cycling treatment in a potential range of −0.2 to 1.0 V at a scan rate of 100 $mV\,s^{-1}$.

Keywords: mesoporous materials · micelle assembly · platinum · polymeric micelles · solvent composition

How to cite: *Angew. Chem. Int. Ed.* **2016**, *55*, 10037 – 10041
Angew. Chem. **2016**, *128*, 10191 – 10195

[1] a) Y. Sakamoto, M. Kaneda, O. Terasaki, D. Zhao, J. M. Kim, G. Stucky, H. J. Shin, R. Ryoo, *Nature* **2000**, *408*, 449 – 453; b) Y. Fang, Y. Lv, J. Tang, H. Wu, D. Jia, D. Feng, B. Kong, Y. Wang, A. A. Elzatahry, D. Al-Dahyan, Q. Zhang, G. Zheng, D. Zhao, *Angew. Chem. Int. Ed.* **2015**, *54*, 8425 – 8429; *Angew. Chem.* **2015**, *127*, 8545 – 8549; c) S. Wang, Q. Zhao, H. Wei, J. Q. Wang, M. Cho, H. S. Cho, O. Terasaki, Y. Wan, *J. Am. Chem. Soc.* **2013**, *135*, 11849 – 11860; d) B. Kong, J. Tang, Y. Zhang, T. Jiang, X. Gong, C. Peng, J. Wei, J. Yang, Y. Wang, X. Wang, G. Zheng, C. Selomulya, D. Zhao, *Nat. Chem.* **2016**, *8*, 171 – 178; e) T. Suteewong, H. Sai, R. Cohen, S. Wang, M. Bradbury, B. Baird, S. M. Gruner, U. Wiesner, *J. Am. Chem. Soc.* **2011**, *133*, 172 – 175.

[2] a) K. C. Kao, C. H. Lin, T. Y. Chen, Y. H. Liu, C. Y. Mou, *J. Am. Chem. Soc.* **2015**, *137*, 3779 – 3782; b) C. Li, B. Jiang, N. Miyamoto, J. H. Kim, V. Malgras, Y. Yamauchi, *J. Am. Chem. Soc.* **2015**, *137*, 11558 – 11561; c) Q. Yue, J. Li, W. Luo, Y. Zhang, A. A. Elzatahry, X. Wang, C. Wang, W. Li, X. Cheng, A. Alghamdi, A. M. Abdullah, Y. Deng, D. Zhao, *J. Am. Chem. Soc.* **2015**, *137*, 13282 – 13289; d) L. Han, K. Miyasaka, O. Terasaki, S. Che, *J. Am. Chem. Soc.* **2011**, *133*, 11524 – 11533.

[3] a) Y. Deng, J. Wei, Z. Sun, D. Zhao, *Chem. Soc. Rev.* **2013**, *42*, 4054 – 4070; b) D. Niu, Z. Liu, Y. Li, X. Luo, J. Zhang, J. Gong, J. Shi, *Adv. Mater.* **2014**, *26*, 4947 – 4953.

[4] J. Wei, H. Wang, Y. Deng, Z. Sun, L. Shi, B. Tu, M. Luqman, D. Zhao, *J. Am. Chem. Soc.* **2011**, *133*, 20369 – 20377.

[5] a) J. Zhang, Y. Deng, J. Wei, Z. Sun, D. Gu, H. Bongard, C. Liu, H. Wu, B. Tu, F. Schüth, D. Zhao, *Chem. Mater.* **2009**, *21*, 3996 – 4005; b) J. Shim, J. Lee, Y. Ye, J. Hwang, S. K. Kim, T. H. Lim, U. Wiesner, J. Lee, *ACS Nano* **2012**, *6*, 6870 – 6881.

[6] a) Y. Deng, T. Yu, Y. Wan, Y. Shi, Y. Meng, D. Gu, L. Zhang, Y. Huang, C. Liu, X. Wu, D. Zhao, *J. Am. Chem. Soc.* **2007**, *129*, 1690 – 1697; b) A. Thomas, H. Schlaad, B. Smarsly, M. Antonietti, *Langmuir* **2003**, *19*, 4455 – 4459.

[7] a) Y. Li, W. Luo, N. Qin, J. Dong, J. Wei, W. Li, S. Feng, J. Chen, J. Xu, A. A. Elzatahry, M. H. Es-Saheb, Y. Deng, D. Zhao, *Angew. Chem. Int. Ed.* **2014**, *53*, 9035 – 9040; *Angew. Chem.* **2014**, *126*, 9181 – 9186; b) E. Ortel, A. Fischer, L. Chuenchom, J. Polte, F. Emmerling, B. M. Smarsly, R. Kraehnert, *Small* **2012**, *8*, 298 – 309.

[8] R. M. Grudzien, J. P. Blitz, S. Pikus, M. Jaroniec, *J. Colloid Interface Sci.* **2009**, *333*, 354 – 362.

[9] a) X. Huang, Y. Li, Y. Chen, E. Zhou, Y. Xu, H. Zhou, X. Duan, Y. Huang, *Angew. Chem. Int. Ed.* **2013**, *52*, 2520 – 2524; *Angew. Chem.* **2013**, *125*, 2580 – 2584; b) L. Wang, Y. Yamauchi, *J. Am. Chem. Soc.* **2009**, *131*, 9152 – 9153; c) C. Li, T. Sato, Y. Yamauchi, *Angew. Chem. Int. Ed.* **2013**, *52*, 8050 – 8053; *Angew. Chem.* **2013**, *125*, 8208 – 8211; d) H. Wang, H. Y. Jeong, M. Imura, L. Wang, L. Radhakrishnan, N. Fujita, T. Castle, O. Terasaki, Y. Yamauchi, *J. Am. Chem. Soc.* **2011**, *133*, 14526 – 14529; e) V. Malgras, H. Ataee-Esfahani, H. Wang, B. Jiang, C. Li, K. C. W. Wu, J. H. Kim, Y. Yamauchi, *Adv. Mater.* **2016**, *28*, 993 – 1010; f) C. Li, B. Jiang, H. Chen, M. Imura, L. Sang, V. Malgras, Y. Bando, T. Ahamad, S. M. Alshehri, S. Tominaka, Y. Yamauchi, *Nano Res.* **2016**, *9*, 1752 – 1762.

[10] a) A. Takai, Y. Yamauchi, K. Kuroda, *J. Am. Chem. Soc.* **2010**, *132*, 208 – 214; b) C. Li, Ö. Dag, T. D. Dao, T. Nagao, Y. Sakamoto, T. Kimura, O. Terasaki, Y. Yamauchi, *Nat. Commun.* **2015**, *6*, 6608.

[11] a) B. Y. Xia, H. B. Wu, N. Li, Y. Yan, X. W. Lou, X. Wang, *Angew. Chem. Int. Ed.* **2015**, *54*, 3797 – 3801; *Angew. Chem.* **2015**, *127*, 3868 – 3872; b) L. Bu, J. Ding, S. Guo, X. Zhang, D. Su, X. Zhu, J. Yao, J. Guo, G. Lu, X. Huang, *Adv. Mater.* **2015**, *27*, 7204 – 7212; c) H. Lv, Z. Xi, Z. Chen, S. Guo, Y. Yu, W. Zhu, Q. Li, X. Zhang, M. Pan, G. Lu, S. Mu, S. Sun, *J. Am. Chem. Soc.* **2015**, *137*, 5859 – 5862; d) J. Mao, Y. Liu, Z. Chen, D. Wang, Y. Li, *Chem. Commun.* **2014**, *50*, 4588 – 4591; e) H. H. Li, S. Y. Ma, Q. Q. Fu, X. J. Liu, L. Wu, S. H. Yu, *J. Am. Chem. Soc.* **2015**, *137*, 7862 – 7868; f) B. Jiang, C. Li, V. Malgras, Y. Bando, Y. Yamauchi, *Chem. Commun.* **2016**, *52*, 1186 – 1189.

[12] a) I. Bannat, K. Wessels, T. Oekermann, J. Rathousky, D. Bahnemann, M. Wark, *Chem. Mater.* **2009**, *21*, 1645 – 1653; b) Y. Li, B. P. Bastakoti, V. Malgras, C. Li, J. Tang, J. H. Kim, Y. Yamauchi, *Angew. Chem. Int. Ed.* **2015**, *54*, 11073 – 11077; *Angew. Chem.* **2015**, *127*, 11225 – 11229.

[13] a) K. Edelmann, M. Janich, E. Hoinkis, W. Pyckhout-Hintzen, S. Höring, *Macromol. Chem. Phys.* **2001**, *202*, 1638 – 1644; b) A. H. Yuwono, Y. Zhang, J. Wang, X. H. Zhang, H. Fan, W. Ji, *Chem. Mater.* **2006**, *18*, 5876 – 5889.

[14] H. Wang, L. Wang, T. Sato, Y. Sakamoto, S. Tominaka, K. Miyasaka, N. Miyamoto, Y. Nemoto, O. Terasaki, Y. Yamauchi, *Chem. Mater.* **2012**, *24*, 1591 – 1598.

[15] a) Ö. Çelik, Ö. Dag, *Angew. Chem. Int. Ed.* **2001**, *40*, 3799 – 3803; *Angew. Chem.* **2001**, *113*, 3915 – 3919; b) C. Albayrak, G. Gülten, Ö. Dag, *Langmuir* **2007**, *23*, 855 – 860; c) A. F. Demirörs, B. E. Eser, Ö. Dag, *Langmuir* **2005**, *21*, 4156 – 4162; d) C. Albayrak, A. M. Soylu, Ö. Dag, *Langmuir* **2008**, *24*, 10592 – 10595; e) Y. Yamauchi, A. Tonegawa, M. Komatsu, H. Wang, L. Wang, Y. Nemoto, N. Suzuki, K. Kuroda, *J. Am. Chem. Soc.* **2012**, *134*, 5100 – 5109.

[16] a) Y. He, Z. Li, P. Simone, T. P. Lodge, *J. Am. Chem. Soc.* **2006**, *128*, 2745 – 2750; b) M. R. Libera, R. F. Egerton, *Polym. Rev.* **2010**, *50*, 321 – 339; c) J. P. Patterson, M. P. Robin, C. Chassenieux, O. Colombani, R. K. O'Reilly, *Chem. Soc. Rev.* **2014**, *43*, 2412 – 2425.

[17] a) E. G. Kelley, T. P. Smart, A. J. Jackson, M. O. Sullivan, T. H. Epps III, *Soft Matter* **2011**, *7*, 7094 – 7102; b) A. H. Yuwono, Y. Zhang, J. Wang, X. H. Zhang, H. Fan, W. Ji, *Chem. Mater.* **2006**, *18*, 5876 – 5889.

[18] a) B. Lim, M. Jiang, P. H. C. Camargo, E. C. Cho, J. Tao, X. Lu, Y. Zhu, Y. Xia, *Science* **2009**, *324*, 1302 – 1305; b) B. Y. Xia, H. B. Wu, Y. Yan, X. W. Lou, X. Wang, *J. Am. Chem. Soc.* **2013**, *135*, 9480 – 9485; c) H. W. Liang, X. Cao, F. Zhou, C. H. Cui, W. J. Zhang, S. H. Yu, *Adv. Mater.* **2011**, *23*, 1467 – 1471; d) L. Dai, S. Mo, Q. Qin, X. Zhao, N. Zheng, *Small* **2016**, *12*, 1572 – 1577.

[19] a) B. Jiang, C. Li, V. Malgras, Y. Yamauchi, *J. Mater. Chem. A* **2015**, *3*, 18053 – 18058; b) J. Ding, X. Zhu, L. Bu, J. Yao, J. Guo, S. Guo, X. Huang, *Chem. Commun.* **2015**, *51*, 9722 – 9725; c) M. Wang, X. Wang, J. Li, L. Liu, *J. Mater. Chem. A* **2013**, *1*, 8127 – 8133.

[20] a) K. Zhang, W. Yang, C. Ma, Y. Wang, C. Sun, Y. Chen, P. Duchesne, J. Zhou, J. Wang, Y. Hu, M. N. Banis, P. Zhang, F. Li, J. Li, L. Chen, *NPG Asia Mater.* **2015**, *7*, 153; b) G. Zhang, C. Huang, R. Qin, Z. Shao, D. An, W. Zhang, Y. Wang, *J. Mater. Chem. A* **2015**, *3*, 5204 – 5211.

[21] a) E. A. Franceschini, G. A. Planes, F. J. Williams, G. J. A. A. Soler-Illia, H. R. Corti, *J. Power Sources* **2011**, *196*, 1723 – 1729; b) B. Jiang, C. Li, M. Imura, J. Tang, Y. Yamauchi, *Adv. Sci.* **2015**, *2*, 1500112; c) Q. Shi, Y. Song, C. Zhu, H. Yang, D. Du, Y. Lin, *ACS Appl. Mater. Interfaces* **2015**, *7*, 24288 – 24295; d) E. A. Franceschini, M. M. Bruno, F. J. Williams, F. A. Viva, H. R. Corti, *ACS Appl. Mater. Interfaces* **2013**, *5*, 10437 – 10444.

[22] a) J. Kibsgaard, Y. Gorlin, Z. Chen, T. F. Jaramillo, *J. Am. Chem. Soc.* **2012**, *134*, 7758 – 7765; b) C. Zhu, D. Du, A. Eychmüller, Y. Lin, *Chem. Rev.* **2015**, *115*, 8896 – 8943; c) B. Jiang, C. Li, V. Malgras, M. Imura, S. Tominaka, Y. Yamauchi, *Chem. Sci.* **2016**, *7*, 1575 – 1581.

Received: April 24, 2016
Revised: May 25, 2016
Published online: July 21, 2016

